ACS OMEGA

Article

Cite This: ACS Omega 2018, 3, 5195−5201

Impact of Pore−Walls Ligand Assembly on the Biodegradation of Mesoporous Organosilica Nanoparticles for Controlled Drug Delivery

Haneen Omar,[†] Basem Moosa,[†] Kholod Alamoudi,[†] Dalaver H. Anjum,[‡] Abdul-Hamid Emwas,[‡] Omar El Tall,[‡] Binh Vu,[§] Fuyu Tamanoi,[§] Abdulaziz AlMalik,*[,∥] and Niveen M. Khashab*[,†]

[†]Smart Hybrid Materials Laboratory, Advanced Membranes, and Porous Materials Center, King Abdullah University of Science and Technology, Thuwal 23955-6900, Saudi Arabia

[‡]King Abdullah University of Science and Technology (KAUST), Core Labs, Thuwal 23955-6900, Saudi Arabia

[§]Department of Microbiology, Immunology and Molecular Genetics, Jonsson Comprehensive Cancer Center, Molecular Biology Institute, University of California, Los Angeles, California 90095-1489, United States

[∥]Life Sciences and Environment Research Institute, Center of Excellence in Nanomedicine (CENM), King Abdulaziz City for Science and Technology (KACST), Riyadh 11461, Saudi Arabia

Supporting Information

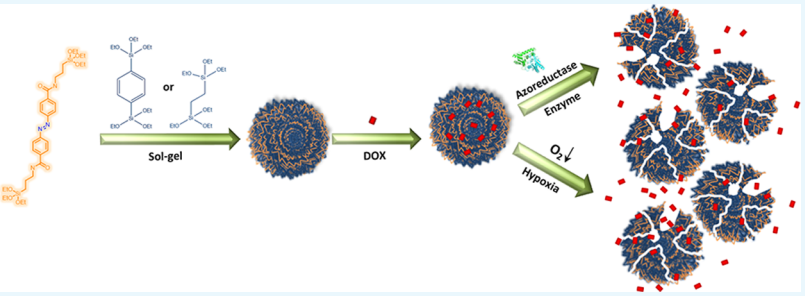

ABSTRACT: Porous materials with molecular-scale ordering have attracted major attention mainly because of the possibility to engineer their pores for selective applications. Periodic mesoporous organosilica is a class of hybrid materials where self-assembly of the organic linkers provides a crystal-like pore wall. However, unlike metal coordination, specific geometries cannot be predicted because of the competitive and dynamic nature of noncovalent interactions. Herein, we study the influence of competing noncovalent interactions in the pore walls on the biodegradation of organosilica frameworks for drug delivery application. These results support the importance of studying self-assembly patterns in hybrid frameworks to better engineer the next generation of dynamic or "soft" porous materials.

1. INTRODUCTION

Controlling periodicity in hybrid porous structures has bestowed infinite practical utilities, especially in the fields of separation, encapsulation, and catalysis.[1−3] The crystalline features of molecularly ordered hybrid structures, such as metal−organic frameworks (MOFs), made these materials quite superior to their amorphous counterparts.[4] Periodic mesoporous organosilica (PMOs) are a class of inorganic−organic hybrid porous materials that have crystal-like pore walls with structural periodicity. It is synthesized by direct condensation of the bridged organosilane precursor $(R'O)_3Si-R-Si(OR')_3$ where R is the organic bridging group.[5−8] Inagaki et al. reported the first periodic organosilica with lamellar ordered pore walls employing a benzene organic bridge.[9] Supramolecular structures formed by self-directed assembly in trans or cis isomers of azobenzene has also been reported.[10−13] More recently, hydrogen bonding in cyclohexane triamide caused a new type of molecular-scale ordering within the pore wall, which improved the guest loading efficiency in these hybrid structures.[5] Engineering ordered porous structures employing noncovalent interactions rather than metal coordination is quite intriguing, as it can produce a new generation of hierarchical and dynamic porous structures especially for biomedical applications.[14]

Many degradable PMOs have been designed that can be triggered by light,[14] enzyme (GTH, trypsin),[15,16] pH,[17] and electrostatic interaction[18] to controllably release the therapeutic cargo. Moreover, loading guest organic molecules in the pores does not need a capping agent because of the hydrophobic interaction between the guest and organic pore wall.[19] Enzymatic triggers are highly thought after because of their selectivity and site specificity.[20,21] The azo-bond is an interesting moiety to employ in a biodegradable drug delivery system, as it reductively cleaves in the presence of azoreductase.[22−25] Moreover, this bond could be effectively cleaved by one-electron reduction which is applicable only

Received: March 6, 2018
Accepted: April 19, 2018
Published: May 14, 2018

DOI: 10.1021/acsomega.8b00418
ACS Omega 2018, 3, 5195−5201

under hypoxia conditions.[26−29] In addition, azoreductase was used as a trigger to visualize specifically lysosomes in hypoxic cancer cells.[30] Many drug delivery systems were reported using this building block as a trigger such as MOFs,[31] polymeric vesicles,[32] and hydrogels.[33]

In this work, we study the influence of ligands self-assembly on the biodegradation of mesoporous organosilica nanoparticles (NPs) for on-demand drug delivery. Azobenzene linkers (AZO) were condensed with aromatic benzene (B) or aliphatic ethane (E), bridging groups to prepare the hybrid frameworks AZO-B and AZO-E, respectively (Figure 1).

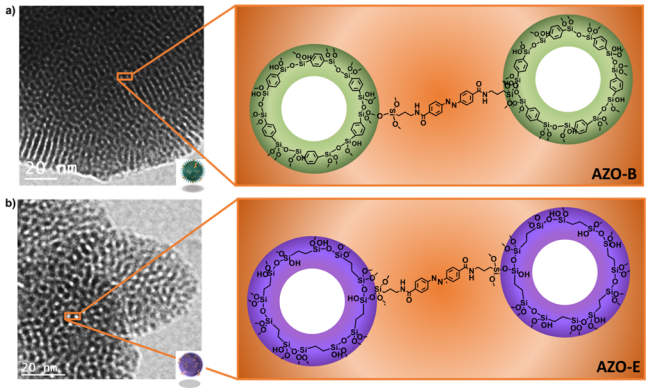

Figure 1. Transmission electron microscopy (TEM) and schematic illustration of (a) AZO-B and (b) AZO-E pore walls.

Investigating the ligand packing on both frameworks showed that AZO-B afforded a framework with a compact pore wall compared with AZO-E. Interestingly, AZO-B showed a faster biodegradation than AZO-E in vitro and in vivo. We expect that other hybrid structures can be produced in a fashion similar to tailor pore wall chemistry and enable the preparation of soft hybrid frameworks with site-specific conjugation and degradation.

2. RESULTS AND DISCUSSION

Polycondensation of diazobenzene-triethoxysilyl amide (165 μL, 0.20 mmol) under basic conditions with benzene (400 μL, 1.0 mmol) or ethane-modified silanes (250 μL, 1.0 mmol) followed by extraction with an alcoholic solution of ammonium nitrate (6 g L^{-1}) and drying overnight afforded NPs AZO-B and AZO-E, respectively. Azobenzene may form multiple noncovalent interactions depending on the neighboring molecules, and the dynamic nature of the azo bond makes it more susceptible to degradation.[34] Increasing the percentage of azobenzene beyond 15% afforded bulk samples at the microscale with a more complex pore wall packing. The AZO linker **1** was prepared following Scheme S1 and fully characterized using ^{1}H and ^{13}C NMR (Figure S1). The TEM images of AZO-B and AZO-E reveal well-ordered arrangements of mesoscopically ordered pores with a hexagonal symmetry (Figures S2a,b and S3a,b, respectively). The chemical composition of AZO-B and AZO-E NPs was confirmed by scanning TEM (STEM) combined with electron energy loss spectroscopy (EELS) and energy dispersive X-ray spectroscopy (EDX) (Figures S2h,i and S3h,i, respectively). The STEM−EELS validated the homogeneous distribution of the azo precursor within AZO-B and AZO-E frameworks by the elemental mappings of silicon, oxygen, nitrogen, and carbon (Figures S2c−g and S3c−g, respectively). EDX spectroscopy also confirmed the presence of silicon, oxygen, carbon, and nitrogen elements (Figures S2i and S3i). Fourier transform infrared spectroscopy (FT-IR) verified the successful incorporation of AZO in the framework of AZO-B where the characteristic peaks of silica [ν_{Si-O} (1090−1125 cm^{-1})][35] and the ν_{C-H} and ν_{Si-C} stretching vibration modes of the benzene group at 3070 and 1162 cm^{-1} were observed (Figure S4).[36] The vibrational spectra of azobenzene were detected in the 1650−900 cm^{-1} region,[37] and the out-of-plane aromatic δ_{Csp^2-H} bending was detected at 534 cm^{-1} (Figure S4). Similarly, FT-IR of AZO-E showed the ethane modes ν_{Si-C} and aliphatic ν_{C-H} at 1162 and 2908 cm^{-1} and the δ_{Csp^2-H} at 918 cm^{-1},[38] along with the stretching mode of ν_{Si-O} from 1090 to 1125 cm^{-1} (Figure S4).[38] Solid-state ^{13}C and ^{29}Si magic angle spinning (MAS) NMR measurements of AZO-B showed a successful incorporation of organic moieties into the mesostructured NPs with a degree of condensation of ca. 70% (Figure 2a). The NMR spectrum of AZO-B shows the peaks at −59, −68, and −77 ppm, corresponding to $T^1(CSi(OSi)(OH)_2)$, $T^2(CSi(OSi)_2(OH))$, and $T^3(CSi(OSi)_3)$, respectively, in addition to a small peak at −108 ppm attributable to $Q^4(Si(OSi)_4)$, suggesting that the condensation has proceeded.[39] The ^{13}C NMR spectrum was dominated by a peak at 135 ppm, which corresponds to the superposition of unresolved signals from o- and m-carbons in the phenylene ring (Figure 2b).[39] There were two additional peaks at 30 and 53 ppm, which were assigned to aliphatic groups (Si−O−CH_2CH_3). The ^{29}Si MAS NMR

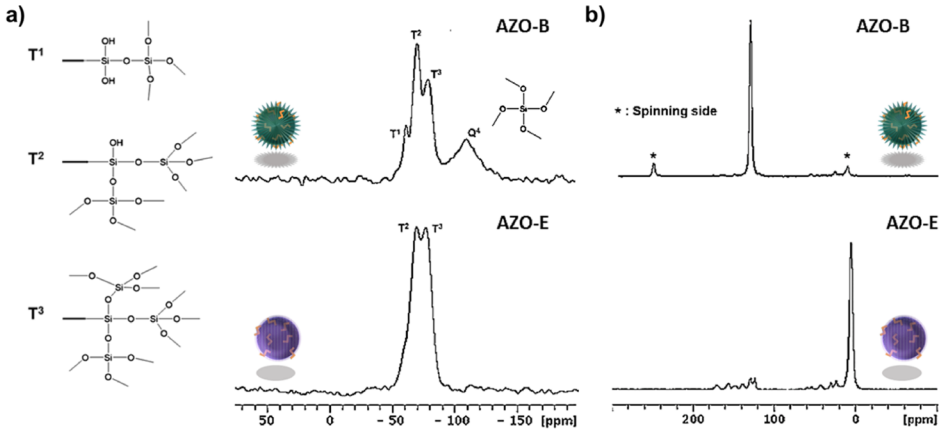

Figure 2. (a) ^{29}Si MAS spectra and (b) ^{13}C CP/MAS NMR spectra of AZO-B and AZO-E.

DOI: 10.1021/acsomega.8b00418
ACS Omega 2018, 3, 5195−5201

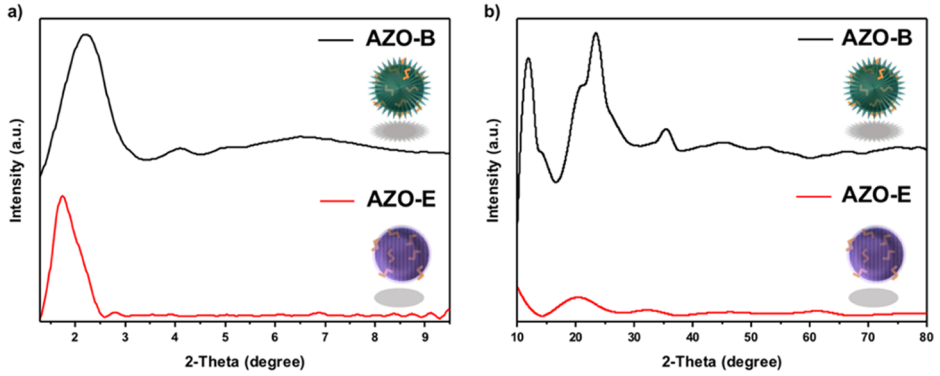

Figure 3. (a) Low- and (b) high-angle XRD patterns of AZO-B and AZO-E samples.

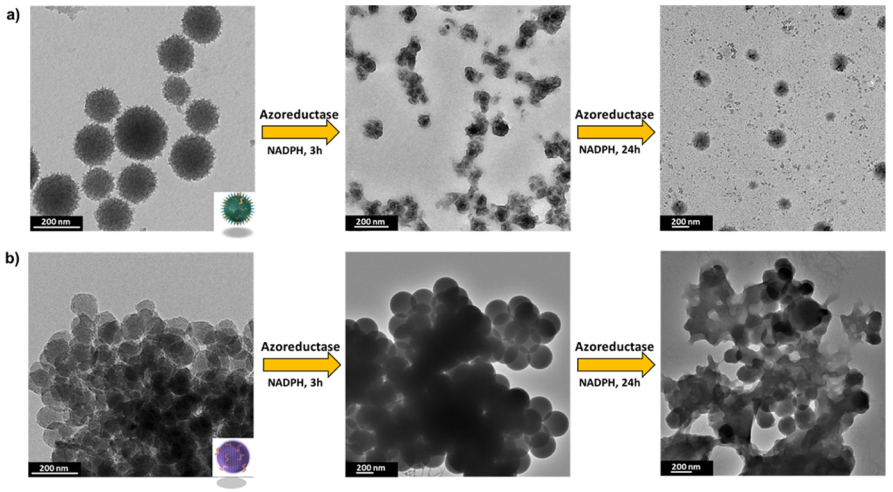

Figure 4. TEM images of (a) AZO-B and (b) AZO-E before and after degradation in azoreductase enzyme in the presence of NADPH for 3 and 24 h.

spectra of AZO-E exhibited two resonances with a degree of condensation of ca. 84% (Figure 2a). The first resonance (−71.6 ppm) was attributed to $T^2(CSi(OSi)_2(OH))$, a partially condensed silica species with one hydroxyl group and the other (−80.7 ppm) was assigned to $T^3(CSi(OSi)_3)$, a fully condensed silicon with three siloxane bonds.[39] Virtually, no peak was detected for SiO_4 species (Si sites attached to four oxygen atoms Q^n, n = 1−4) between −98 and −111 ppm, indicating essentially no evidence for Si−C bond cleavage during the sol−gel processing and synthesis.[40] The ^{13}C MAS NMR spectrum showed the presence of a signal at 5 ppm (Figure 2b). This is due to the $-CH_2-CH_2-$ groups covalently linked to two Si atoms.[41,42]

XRD analysis was performed to study the structure arrangement and phase purity of the AZO NPs. The low-angle XRD patterns for AZO-B and AZO-E show dominant diffraction peaks (100) at 2θ = 2.2 with a spacing of d = 4.02 nm and 2θ = 1.74 with a spacing of d = 5.08 nm, indicating a two-dimensional hexagonal symmetry (*p6mm*) of the materials (Figure 3).[43] The corresponding lattice constants of the (100) reflection were found to be 4.65 nm for AZO-B and 5.87 nm for AZO-E, which support the mesoscale-periodicity of the NPs.[9,43] AZO-B low-angle XRD spectrum shows two additional diffraction peaks, which can be indexed as (110) and (200) reflections as shown in Figure 3a. The high-angle XRD patterns of AZO-B displayed additional three diffraction peaks at 2θ = 11.6°, 23.4°, and 35.4° which equates to d = 0.76, 0.38, and 0.25 nm, respectively (Figure 3b).

Nitrogen adsorption−desorption of AZO-B and AZO-E showed type IV isotherm, which is characteristic of a mesoporous material (Figure S5).[44] The structural information on both systems is listed in Table S1. The AZO-B-specific surface area, pore volume, and pore size were 1211 m^2/g, 0.84 cm^3/g, and 1.6 nm, respectively. The AZO-E shows an increase in the pore size to 2.7 nm, but the specific surface area and pore volume are comparable to AZO-B (1190 m^2/g and 0.85 cm^3/g, respectively). These results suggest that the AZO linker plays a significant role in controlling the pore size of the NPs. The pore size distribution of the materials was obtained by the Barrett−Joyner−Halenda method.[45] Both samples have uniform pore size distributions with a dominant peak center at 1.6 nm for AZO-B and 2.7 nm for AZO-E, which is in agreement with the pore dimensions estimated from the high-resolution TEM images. The measured pore width by TEM was about 2−3 nm, which is in good agreement with the nitrogen isotherm results.

Biodegradation of NPs has recently become a hot research topic because of the impact of these lingering nanoplatforms on the environment and general health. Hundreds of nano-formulations exist in the market predominantly in the personal care and cosmetics industry. Crystallinity and order in these systems have proved crucial for their toxicity and consequently intended use.[46] Targeted drug delivery is also an important application of enzymatically degradable NPs.[47] We thus tested

DOI: 10.1021/acsomega.8b00418
ACS Omega 2018, 3, 5195−5201

the biodegradation of AZO-B and AZO-E to verify the effect on decomposition. Mimicking a reducing tumor microenvironment, a biological media containing the azoreductase enzyme in the presence of coenzyme NADPH was used in this study. Azoreductase can reductively cleave the azo-bond and has been used enormously in colon-specific drug delivery systems such as a prodrug sulfasalazine.[48−55] The biodegradation of AZO-B and AZO-E in the azoreductase enzyme was monitored by TEM over a period of 24 h (Figure 4). Interestingly, AZO-B degraded faster than AZO-E, which may be attributed to the relatively smaller pores. Although such assemblies are considered more stable, the close proximity of bonds interacting with the active site of the azoreductase enzyme might be enhancing the rate of biodegradation.

We then tested biocompatibility and the utility of such system in targeted drug delivery. Colon cancer cells, HCT-116 cells, were used for all in vitro testings. Both AZO-B and AZO-E exhibit no significant cytotoxicity against HCT-116 cells at a high concentration of 100 μg/mL (Figure 5). However, AZO-E showed a safer profile where 95% of the cells were viable at a NP concentration of 100 μg/mL compared with 60% when AZO-B was used.

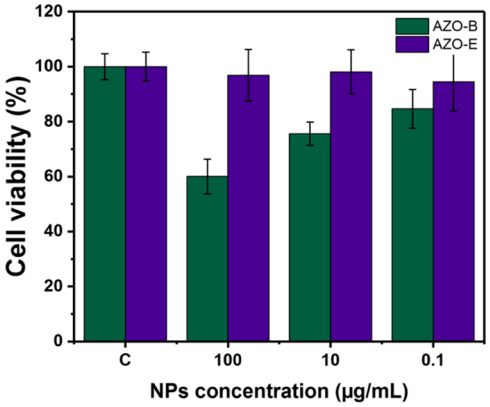

Figure 5. Cell viability in colon cancer (HCT-116) cells of AZO-B and AZO-E.

Both systems were then loaded with the anticancer drug doxorubicin (DOX) and tested in physiological media before in vitro incubation with HCT-116 cells. The release experiments were carried out in the presence and absence of the azoreductase enzyme and NADPH coenzyme. Figure 6a shows that DOX release was initiated by the presence of the azoreductase enzyme. A negligible amount of DOX was released in the absence of the enzyme, and the system was not leaking as can be concluded from the release profile (Figure 6a). DOX was efficiently loaded in AZO-NPs, and incubation of AZO-B and AZO-E with HCT-116 cells showed efficient uptake and delivery of DOX into cancer cells under hypoxic conditions (Figure 6b). Confocal laser scanning microscopy (CLSM) images showed an increase in red fluorescence of DOX molecules when AZO-NPs are used, which is in agreement with the drug release profile that showed a higher drug release profile for AZO-B compared with AZO-E. Furthermore, 3D intracellular fluorescence reconstruction of the uptake and delivery is presented in Figure S6. As a control, AZO-B and AZO-E were incubated with HCT-116 cells in the absence nonhypoxic conditions and showed no drug release because of negligible amounts of NP degradation.

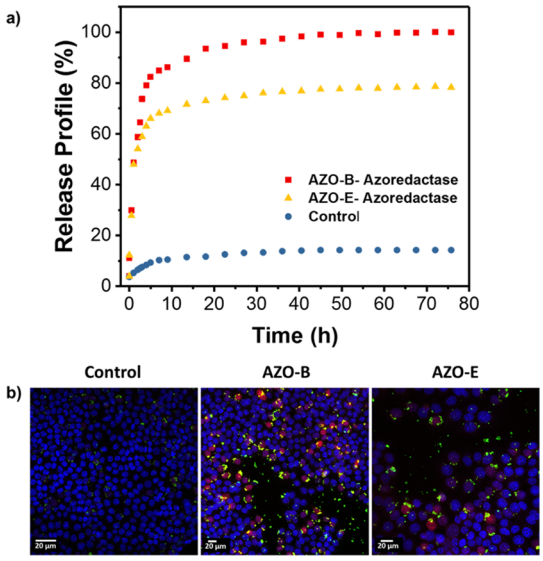

Figure 6. (a) DOX release profiles of AZO-B and AZO-E in the absence and presence of the azoreductase enzyme. (b) CLSM images of HCT-116 cells incubated with DOX loaded AZO-B and AZO-E under hypoxia for 1 h. Nuclei are stained in blue with Hoechst 33342 dye, NPs appear with the green fluorescence (fluorescein isothiocyanate) and DOX fluorescence in cells (red).

Chicken embryos were transplanted with OVCAR-8 ovarian cancer cells, expressing green fluorescent protein. Loaded NPs with DOX were injected into the blood vessels followed by daily monitoring of tumor sizes relative to controls. Figure 7

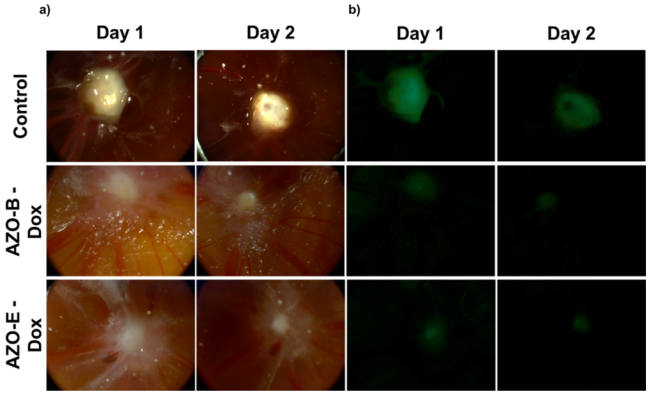

Figure 7. (a) Actual and (b) visible light fluorescence images of chicken egg tumor transplanted with OVCAR-8 cells before and after injection with DOX-loaded AZO-B and AZO-E.

shows that the injection of drug-loaded NPs has potent antitumor activity without any other toxic effects on organs. Administration of NPs loaded with DOX results in a dramatic tumor shrinkage relative to control over time. AZO-B showed a drastic decrease in the tumor size just after two days of injection compared with AZO-E, while safely retaining the function of all other organs.

3. CONCLUSION

Studying pore wall packing will lead to interesting hybrid platforms that can be smart in nature. This molecular scale ordering will drastically influence the properties of these frameworks. Engineering materials to have a different pore size is well established. However, we need to investigate the overall

DOI: 10.1021/acsomega.8b00418
ACS Omega 2018, 3, 5195−5201

properties of these materials, especially when it comes to stability and responsiveness. In this work, we showed that closer pore packing in AZO-B enhanced the enzymatic biodegradation of these hybrid frameworks compared with AZO-E. Understanding pore wall packing and assembly of linkers within the space will lead to superior porous materials that can make it closer to scale-up and eventual market use.

4. EXPERIMENTAL SECTION

4.1. Materials and Methods. Cetyltrimethylammonium bromide (CTAB), 1,4-bis(triethoxysilyl)benzene, 1,2-bis-(trimethoxysilyl)ethane, 4-nitrobenzoic acid, glucose, thionyl chloride, tetrahydrofuran [THF; anhydrous, ≥99.9% (dry THF)], trimethylamine, and 3-aminopropyltriethoxysilane were purchased from Sigma-Aldrich. Sodium hydroxide (NaOH) and phosphate buffered saline [(10×), pH 7.4] were purchased from Fisher. Milli-Q water was used in all synthetic experiments. All chemicals were used without further purification.

4.2. Instrumentation. Powder XRD measurements were performed using a PANalytical X'Pert Pro X-ray powder diffractometer using the Cu Kα radiation (40 V, 40 mA, λ = 1.54056 Å) in a θ–θ mode from 20° to 90° (2θ). TEM images, EELS, and EDX were recorded using a Tecnai 12 T (FEI Co.) microscope operated at 120 kV. The GIF was used in the EELS mode in conjunction with high angle annular dark field–STEM. Nitrogen adsorption–desorption isotherms were acquired using a Micromeritics ASAP 2420 instrument. ^{1}H NMR and ^{13}C NMR spectra were performed at 500 MHz with $CDCl_3$ solutions with an AVANCE III Bruker Corporation instrument. For solid NMR spectra were carried out by using a Bruker 400 MHz AVANCE III NMR spectrometer (resonating at 100.64 MHz for ^{13}C and 79.514 MHz for ^{29}Si) equipped with double resonance 4 mm Bruker MAS probe (Bruker BioSpin, Rheinstetten, Germany). To be able to spin the samples were finely ground then packed evenly into 4 mm zirconia rotor and sealed at the open end with a Vespel cap. The ^{29}Si spectra were recorded with 14 kHz spinning rate using one pulse program from Bruker standard pulse library with 30° flipping angle with recycle delay time of 30 s. The ^{13}C spectra were recorded using cross polarization CP MAS experiments using the CP pulse program. Each ^{13}C NMR spectrum was recorded by collecting 12k scans while the ^{29}Si NMR spectrum was recorded with 4k scans at room temperature. Bruker Topspin 3.2 software (Bruker BioSpin, Rheinstetten, Germany) was used for data collection and analysis. FT-IR spectra were recorded using a Thermo Scientific spectrometer (Nicolet iS10). Absorption spectra were recorded using a Varian Cary 5000 spectrophotometer, and fluorescence data were collected using a Varian Cary Eclipse fluorimeter.

4.3. Synthesis of AZO-B and AZO-E NPs. A mixture of CTAB (250 mg, 0.68 mmol), distilled water (120 mL), and NaOH (875 μL, 2 M) was stirred at 85 °C for 30 min in a 250 mL round-bottom flask. The azo precursor (165 μL, 0.20 mmol) was added to the solution, followed by 1,4-bis-(triethoxysilyl)benzene (400 μL, 1.0 mmol), and the condensation process was conducted for 2 h at 85 °C. After that, the solution was cooled to room temperature under stirring. The sample was then extracted by using an ultrasonic bath with an alcoholic solution of ammonium nitrate (6 g L^{-1}) at 45 °C for 30 min and washed three times with ethanol, water, and ethanol. The as-prepared material was dried under vacuum. The synthesis of AZO-E NPs was synthesized as described for the AZO-B NPs above with an 1,2-bis-(trimethoxysilyl)ethane precursor (250 μL, 1.0 mmol) instead of the 1,4-bis(triethoxysilyl)benzene precursor.

■ ASSOCIATED CONTENT

Supporting Information

The Supporting Information is available free of charge on the ACS Publications website at DOI: 10.1021/acsomega.8b00418.

Detailed procedures for the preparation of AZO precursor, loading, release profile, in vitro and in vivo studies, and all characterization techniques (PDF)

■ AUTHOR INFORMATION

Corresponding Authors

*E-mail: aalmalik@kacst.edu.sa (A.A.).
*E-mail: niveen.khashab@kaust.edu.sa (N.M.K.).

ORCID

Basem Moosa: 0000-0002-2350-4100
Niveen M. Khashab: 0000-0003-2728-0666

Notes

The authors declare no competing financial interest.

■ REFERENCES

(1) Jin, X.; Kang, S.; Tanaka, S.; Park, S. Monitoring the Glutathione Redox Reaction in Living Human Cells by Combining Metabolic Labeling with Heteronuclear NMR. *Angew. Chem., Int. Ed.* **2016**, *55*, 7939–7942.

(2) Du, X.; Li, X.; Xiong, L.; Zhang, X.; Kleitz, F.; Qiao, S. Z. Mesoporous silica nanoparticles with organo-bridged silsesquioxane framework as innovative platforms for bioimaging and therapeutic agent delivery. *Biomaterials* **2016**, *91*, 90–127.

(3) Lin, C. X.; Qiao, S. Z.; Yu, C. Z.; Ismadji, S.; Lu, G. Q. Periodic mesoporous silica and organosilica with controlled morphologies as carriers for drug release. *Microporous Mesoporous Mater.* **2009**, *117*, 213–219.

(4) Eddaoudi, M.; Kim, J.; Rosi, N.; Vodak, D.; Wachter, J.; O'Keeffe, M.; Yaghi, O. M. Systematic Design of Pore Size and Functionality in Isoreticular MOFs and Their Application in Methane Storage. *Science* **2002**, *295*, 469–472.

(5) Mizoshita, N.; Inagaki, S. Periodic Mesoporous Organosilica with Molecular-Scale Ordering Self-Assembled by Hydrogen Bonds. *Angew. Chem., Int. Ed.* **2015**, *54*, 11999–12003.

(6) López, M. I.; Esquivel, D.; Jiménez-Sanchidrián, C.; Romero-Salguero, F. J.; Van Der Voort, P. A "one-step" sulfonic acid PMO as a recyclable acid catalyst. *J. Catal.* **2015**, *326*, 139–148.

(7) Vercaemst, C.; de Jongh, P. E.; Meeldijk, J. D.; Goderis, B.; Verpoort, F.; Van Der Voort, P. Ethenylene-bridged periodic mesoporous organosilicas with ultra-large mesopores. *Chem. Commun.* **2009**, *27*, 4052–4054.

(8) Mizoshita, N.; Tani, T.; Shinokubo, H.; Inagaki, S. Mesoporous Organosilica Hybrids Consisting of Silica-Wrapped π–π Stacking Columns. *Angew. Chem.* **2012**, *124*, 1182–1186.

(9) Inagaki, S.; Guan, S.; Ohsuna, T.; Terasaki, O. An ordered mesoporous organosilica hybrid material with a crystal-like wall structure. *Nature* **2002**, *416*, 304–307.

(10) Liu, N.; Yu, K.; Smarsly, B.; Dunphy, D. R.; Jiang, Y.-B.; Brinker, C. J. Self-directed assembly of photoactive hybrid silicates derived from an azobenzene-bridged silsesquioxane. *J. Am. Chem. Soc.* **2002**, *124*, 14540–14541.

(11) Liu, N.; Chen, Z.; Dunphy, D. R.; Jiang, Y.-B.; Assink, R. A.; Brinker, C. J. Photoresponsive Nanocomposite Formed by Self-Assembly of an Azobenzene-Modified Silane. *Angew. Chem., Int. Ed.* **2003**, *42*, 1731–1734.

(12) Wei, J.; Liu, Y.; Chen, J.; Li, Y.; Yue, Q.; Pan, G.; Yu, Y.; Deng, Y.; Zhao, D. Azobenzene-Derived Surfactants as Phototriggered

DOI: 10.1021/acsomega.8b00418
ACS Omega 2018, 3, 5195–5201

Recyclable Templates for the Synthesis of Ordered Mesoporous Silica Nanospheres. *Adv. Mater.* **2014**, *26*, 1782−1787.
(13) Angelos, S.; Choi, E.; Vögtle, F.; De Cola, L.; Zink, J. I. Photo-driven expulsion of molecules from mesostructured silica nanoparticles. *J. Phys. Chem. C* **2007**, *111*, 6589−6592.
(14) Kapoor, M. P.; Yang, Q.; Inagaki, S. Self-assembly of biphenylene-bridged hybrid mesoporous solid with molecular-scale periodicity in the pore walls. *J. Am. Chem. Soc.* **2002**, *124*, 15176−15177.
(15) Fatieiev, Y.; Croissant, J. G.; Alsaiari, S.; Moosa, B. A.; Anjum, D. H.; Khashab, N. M. Photoresponsive bridged silsesquioxane nanoparticles with tunable morphology for light-triggered plasmid DNA delivery. *ACS Appl. Mater. Interfaces* **2015**, *7*, 24993−24997.
(16) Omar, H.; Croissant, J. G.; Alamoudi, K.; Alsaiari, S.; Alradwan, I.; Majrashi, M. A.; Anjum, D. H.; Martins, P.; Laamarti, R.; Eppinger, J.; Moosa, B.; Almalik, A.; Khashab, N. M. Biodegradable Magnetic Silica@Iron Oxide Nanovectors with Ultra-Large Mesopores for High Protein Loading, Magnetothermal Release, and Delivery. *J. Controlled Release* **2017**, *259*, 187−194.
(17) Fertier, L.; Théron, C.; Carcel, C.; Trens, P.; Man, M. W. C. pH-Responsive Bridged Silsesquioxane. *Chem. Mater.* **2011**, *23*, 2100−2106.
(18) Li, S.; Moosa, B. A.; Croissant, J. G.; Khashab, N. M. Electrostatic Assembly/Disassembly of Nanoscaled Colloidosomes for Light-Triggered Cargo Release. *Angew. Chem.* **2015**, *127*, 6908−6912.
(19) Wang, W.; Lofgreen, J. E.; Ozin, G. A. Why PMO? Towards functionality and utility of periodic mesoporous organosilicas. *Small* **2010**, *6*, 2634−2642.
(20) Rubinstein, A. Colonic drug delivery. *Drug Discovery Today: Technol.* **2005**, *2*, 33−37.
(21) Roldo, M.; Barbu, E.; Brown, J. F.; Laight, D. W.; Smart, J. D.; Tsibouklis, J. Azo compounds in colon-specific drug delivery. *Expert Opin. Drug Delivery* **2007**, *4*, 547−560.
(22) Ito, K.; Nakanishi, M.; Lee, W.-C.; Zhi, Y.; Sasaki, H.; Zenno, S.; Saigo, K.; Kitade, Y.; Tanokura, M. Expansion of substrate specificity and catalytic mechanism of azoreductase by X-ray crystallography and site-directed mutagenesis. *J. Biol. Chem.* **2008**, *283*, 13889−13896.
(23) Ito, K.; Nakanishi, M.; Lee, W.-C.; Sasaki, H.; Zenno, S.; Saigo, K.; Kitade, Y.; Tanokura, M. Three-dimensional structure of AzoR from Escherichia coli An oxidereductase conserved in microorganisms. *J. Biol. Chem.* **2006**, *281*, 20567−20576.
(24) Rao, J.; Khan, A. Enzyme sensitive synthetic polymer micelles based on the azobenzene motif. *J. Am. Chem. Soc.* **2013**, *135*, 14056−14059.
(25) Rao, J.; Hottinger, C.; Khan, A. Enzyme-Triggered Cascade Reactions and Assembly of Abiotic Block Copolymers into Micellar Nanostructures. *J. Am. Chem. Soc.* **2014**, *136*, 5872−5875.
(26) Wilson, W. R.; Hay, M. P. Targeting hypoxia in cancer therapy. *Nat. Rev. Cancer* **2011**, *11*, 393−410.
(27) Perche, F.; Biswas, S.; Wang, T.; Zhu, L.; Torchilin, V. P. Hypoxia-Targeted siRNA Delivery. *Angew. Chem.* **2014**, *126*, 3430−3434.
(28) Lendahl, U.; Lee, K. L.; Yang, H.; Poellinger, L. Generating specificity and diversity in the transcriptional response to hypoxia. *Nat. Rev. Genet.* **2009**, *10*, 821.
(29) Kiyose, K.; Hanaoka, K.; Oushiki, D.; Nakamura, T.; Kajimura, M.; Suematsu, M.; Nishimatsu, H.; Yamane, T.; Terai, T.; Hirata, Y.; Nagano, T. Hypoxia-Sensitive Fluorescent Probes for in Vivo Real-Time Fluorescence Imaging of Acute Ischemia. *J. Am. Chem. Soc.* **2010**, *132*, 15846−15848.
(30) Luo, S.; Liu, Y.; Wang, F.; Fei, Q.; Shi, B.; An, J.; Zhao, C.; Tung, C.-H. A fluorescent turn-on probe for visualizing lysosomes in hypoxic tumor cells. *Analyst* **2016**, *141*, 2879−2882.
(31) Levine, D. J.; Runčevski, T. e.; Kapelewski, M. T.; Keitz, B. K.; Oktawiec, J.; Reed, D. A.; Mason, J. A.; Jiang, H. Z. H.; Colwell, K. A.; Legendre, C. M. Olsalazine-Based Metal−Organic Frameworks as Biocompatible Platforms for H2 Adsorption and Drug Delivery. *J. Am. Chem. Soc.* **2016**, *138*, 10143−10150.
(32) Gu, W.-X.; Li, Q.-L.; Lu, H.; Fang, L.; Chen, Q.; Yang, Y.-W.; Gao, H. Construction of stable polymeric vesicles based on azobenzene and beta-cyclodextrin grafted poly (glycerol methacrylate) s for potential applications in colon-specific drug delivery. *Chem. Commun.* **2015**, *51*, 4715−4718.
(33) Li, X.; Li, J.; Gao, Y.; Kuang, Y.; Shi, J.; Xu, B. Molecular nanofibers of olsalazine form supramolecular hydrogels for reductive release of an anti-inflammatory agent. *J. Am. Chem. Soc.* **2010**, *132*, 17707−17709.
(34) Lin, Y.; Wang, A.; Qiao, Y.; Gao, C.; Drechsler, M.; Ye, J.; Yan, Y.; Huang, J. Rationally designed helical nanofibers via multiple non-covalent interactions: fabrication and modulation. *Soft Matter* **2010**, *6*, 2031−2036.
(35) Sanaeishoar, H.; Sabbaghan, M.; Mohave, F. Synthesis and characterization of micro-mesoporous MCM-41 using various ionic liquids as co-templates. *Microporous Mesoporous Mater.* **2015**, *217*, 219−224.
(36) Prabavathi, N.; Nayaki, N. S.; Krishnakumar, V. Spectroscopic investigation (FT-IR, FT-Raman, NMR and UV-Vis), conformational stability, NBO and thermodynamic analysis of 1-(2-methoxyphenyl) piperazine and 1-(2-chlorophenyl) piperazine by DFT approach. *Pharm. Anal. Acta* **2015**, *6*, 2.
(37) Tecklenburg, M. M. J.; Kosnak, D. J.; Bhatnagar, A.; Mohanty, D. K. Vibrational characterization of azobenzenes, azoxybenzenes and azoaromatic and azoxyaromatic polyethers. *J. Raman Spectrosc.* **1997**, *28*, 755−763.
(38) Hoffmann, F.; Güngerich, M.; Klar, P. J.; Fröba, M. Vibrational Spectroscopy of Periodic Mesoporous Organosilicas (PMOs) and Their Precursors: A Closer Look. *J. Phys. Chem. C* **2007**, *111*, 5648−5660.
(39) Kapoor, M. P.; Yang, Q.; Inagaki, S. Organization of Phenylene-Bridged Hybrid Mesoporous Silisesquioxane with a Crystal-like Pore Wall from a Precursor with Nonlinear Symmetry. *Chem. Mater.* **2004**, *16*, 1209−1213.
(40) Wei, Y.; Li, X.; Zhang, R.; Liu, Y.; Wang, W.; Ling, Y.; El-Toni, A. M.; Zhao, D. Periodic Mesoporous Organosilica Nanocubes with Ultrahigh Surface Areas for Efficient CO2 Adsorption. *Sci. Rep.* **2016**, *6*, 20769.
(41) Cho, E.-B.; Kim, D.; Jaroniec, M. Periodic Mesoporous Organosilicas with Multiple Bridging Groups and Spherical Morphology. *Langmuir* **2007**, *23*, 11844−11849.
(42) Mohanty, P.; Linn, N. M. K.; Landskron, K. Ultrafast Sonochemical Synthesis of Methane and Ethane Bridged Periodic Mesoporous Organosilicas. *Langmuir* **2010**, *26*, 1147−1151.
(43) Morell, J.; Wolter, G.; Fröba, M. Synthesis and Characterization of Highly Ordered Thiophene-Bridged Periodic Mesoporous Organosilicas with Large Pores. *Chem. Mater.* **2005**, *17*, 804−808.
(44) ALOthman, Z. A Review: Fundamental Aspects of Silicate Mesoporous Materials. *Materials* **2012**, *5*, 2874.
(45) Kruk, M.; Jaroniec, M. Gas Adsorption Characterization of Ordered Organic−Inorganic Nanocomposite Materials. *Chem. Mater.* **2001**, *13*, 3169−3183.
(46) Hussain, S. M.; Braydich-Stolle, L. K.; Schrand, A. M.; Murdock, R. C.; Yu, K. O.; Mattie, D. M.; Schlager, J. J.; Terrones, M. Toxicity Evaluation for Safe Use of Nanomaterials: Recent Achievements and Technical Challenges. *Adv. Mater.* **2009**, *21*, 1549−1559.
(47) Prasetyanto, E. A.; Bertucci, A.; Septiadi, D.; Corradini, R.; Castro-Hartmann, P.; De Cola, L. Breakable Hybrid Organosilica Nanocapsules for Protein Delivery. *Angew. Chem., Int. Ed.* **2016**, *55*, 3323−3327.
(48) Popat, A.; Ross, B. P.; Liu, J.; Jambhrunkar, S.; Kleitz, F.; Qiao, S. Z. Enzyme-Responsive Controlled Release of Covalently Bound Prodrug from Functional Mesoporous Silica Nanospheres. *Angew. Chem., Int. Ed.* **2012**, *51*, 12486−12489.
(49) Navath, S.; Rao, V.; Woodford, R.-M. T.; Midura-Kiela, M. T.; Ahad, A. M.; Alleti, R.; Kiela, P. R.; Mash, E. A. Design, Synthesis, and Testing of a Molecular Truck for Colonic Delivery of 5-Aminosalicylic Acid. *ACS Med. Chem. Lett.* **2012**, *3*, 710−714.

DOI: 10.1021/acsomega.8b00418
ACS Omega 2018, 3, 5195−5201

(50) Wiwattanapatapee, R.; Lomlim, L.; Saramunee, K. Dendrimers conjugates for colonic delivery of 5-aminosalicylic acid. *J. Controlled Release* **2003**, *88*, 1−9.
(51) Lee, C.-H.; Lo, L.-W.; Mou, C.-Y.; Yang, C.-S. Synthesis and Characterization of Positive-Charge Functionalized Mesoporous Silica Nanoparticles for Oral Drug Delivery of an Anti-Inflammatory Drug. *Adv. Funct. Mater.* **2008**, *18*, 3283−3292.
(52) Fujita, S.; Inagaki, S. Self-Organization of Organosilica Solids with Molecular-Scale and Mesoscale Periodicities. *Chem. Mater.* **2008**, *20*, 891−908.
(53) Klotz, U.; Schwab, M. Topical delivery of therapeutic agents in the treatment of inflammatory bowel disease. *Adv. Drug Delivery Rev.* **2005**, *57*, 267−279.
(54) Friend, D. R. Colon-specific drug delivery. *Adv. Drug Delivery Rev.* **1991**, *7*, 149−199.
(55) Friend, D. R. New oral delivery systems for treatment of inflammatory bowel disease. *Adv. Drug Delivery Rev.* **2005**, *57*, 247−265.

DOI: 10.1021/acsomega.8b00418
ACS Omega 2018, 3, 5195−5201